Kondo screening in a charge-insulating spinon metal

M. Gomilšek,[1,2] R. Žitko,[1,3] M. Klanjšek,[1] M. Pregelj,[1] C. Baines,[4] Y. Li,[5] Q. M. Zhang,[6,7] and A. Zorko[1,*]

[1]*Jožef Stefan Institute, Jamova c. 39, SI-1000 Ljubljana, Slovenia*
[2]*Centre for Materials Physics, Durham University, South Road, Durham, DH1 3LE, UK*
[3]*Faculty of Mathematics and Physics, University of Ljubljana, Jadranska c. 19, SI-1000 Ljubljana, Slovenia*
[4]*Laboratory for Muon Spin Spectroscopy, Paul Scherrer Institute, CH-5232 Villigen PSI, Switzerland*
[5]*Experimental Physics VI, Center for Electronic Correlations and Magnetism,*
University of Augsburg, 86159 Augsburg, Germany
[6]*National Laboratory for Condensed Matter Physics and Institute of Physics,*
Chinese Academy of Sciences, Beijing 100190, China
[7]*School of Physical Science and Technology, Lanzhou University, Lanzhou 730000, China*
(Dated: April 16, 2019)

The Kondo effect, an eminent manifestation of many-body physics in condensed matter, is traditionally explained as exchange scattering of conduction electrons on a spinful impurity in a metal [1, 2]. The resulting screening of the impurity's local moment by the electron Fermi sea is characterized by a Kondo temperature T_K, below which the system enters a non-perturbative strongly-coupled regime. In recent years, this effect has found its realizations beyond the bulk-metal paradigm in many other itinerant-electron systems, such as quantum dots in semiconductor heterostructures [3, 4] and in nanomaterials [5–7], quantum point contacts [8, 9], and graphene [10]. Here we report on the first experimental observation of the Kondo screening by chargeless quasiparticles. This occurs in a charge-insulating quantum spin liquid, where spinon excitations forming a Fermi surface take the role of conduction electrons. The observed impurity behaviour therefore bears a strong resemblance to the conventional case in a metal. The discovered spinon-based Kondo effect provides a prominent platform for characterising and possibly manipulating enigmatic host spin liquids.

The Kondo screening of a magnetic impurity embedded in a quantum spin liquid (Fig. 1), a highly-quantum-entangled yet magnetically disordered state where charge degrees of freedom are frozen, has been the subject of theoretical investigations for more than two decades [11–17]. In this case, the itinerant electrons of the standard Kondo picture are effectively replaced by emergent fractional magnetic excitations, inherent to any spin liquid. Due to a large variety of essentially different low-energy excitations, spin liquids should be particularly versatile hosts of Kondo physics. In the case of spinon excitations with a Fermi surface — a spinon metal — a Kondo-like effect similar to the one in an ordinary metal is expected [13, 15]. However, emergent gauge fields mediating spinon–spinon interactions could cause deviations from the generic Fermi-liquid Kondo behaviour. As the spin-liquid Kondo effect has not yet been conclusively

confirmed by experiment, these theoretical predictions remain to be verified.

Zn-brochantite, $ZnCu_3(OH)_6SO_4$, is a particularly well-suited compound for investigating the Kondo effect in a spin liquid. This quantum kagome antiferromagnet [2] is one of only a few examples where a spin-liquid state remains stable down to the lowest experimentally
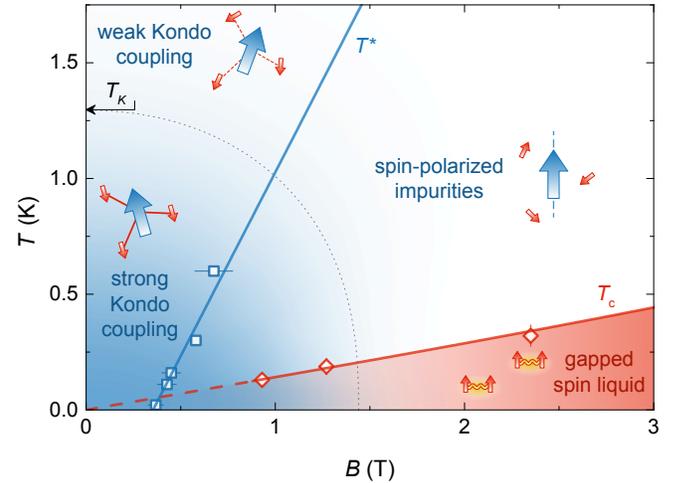
Phase diagram of Zn-brochantite. Kondo screening of impurity spins (large arrows) by spinons (small arrows) in the spin-liquid state of Zn-brochantite, with the Kondo temperature $T_K = 1.3$ K. The intensity of the blue hue indicates the slope of the imaginary part of the dynamical impurity spin susceptibility $\chi''(\omega)/\omega$ at frequency $\omega \to 0$. The dotted line marks the contour corresponding to the value at T_K and $B = 0$. The temperature T^* denotes the crossover between the low-field-Kondo regime and the field-polarized state after Kondo-resonance splitting (the field direction is indicated by the vertical dashed line). $T^*(B)$ yields the g factor $g = 2.3(3)$. The spinon metal undergoes an intrinsic field-induced spinon-pairing transition into a gapped spin-liquid state below a field-dependent critical temperature T_c, where the density of spinon pairs increases with the applied field (red hue) [18]. This instability, which is analogous to the formation of Cooper pairs in superconductors, is characterized by an order of magnitude smaller effective g factor, which clearly differentiates between the two effects.
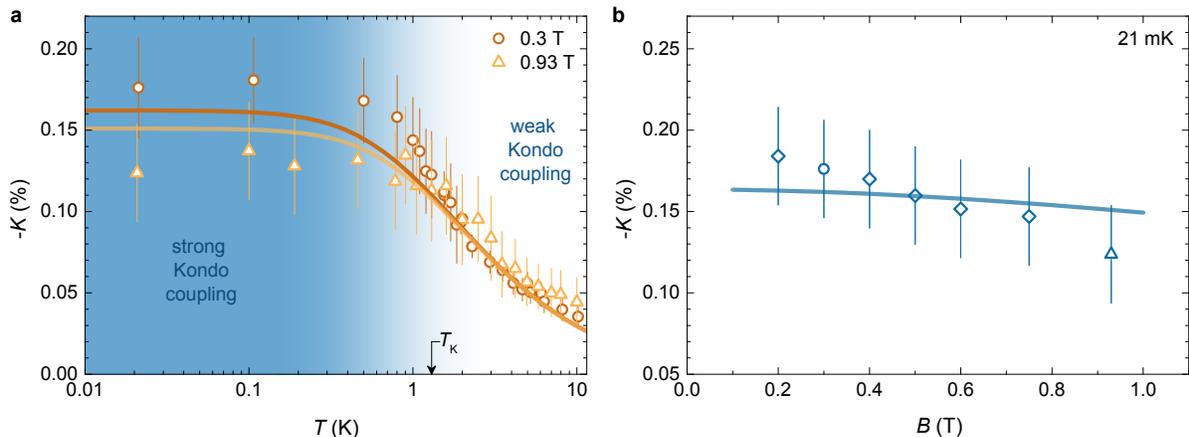
Static μSR signature of the Kondo effect. a, The temperature dependence of the muon Knight shift K (symbols) at two transverse magnetic fields in both the strong-Kondo-coupling (blue region) and the weak-Kondo-coupling regimes. The dataset at 0.3 T corresponds to previously published measurements [22] with a refined analysis (see Methods). The lines show NRG theoretical predictions for the Kondo effect of impurities with concentration $p = 11(2)\%$ coupled to non-interacting spin-1/2 fermions with the magnetic coupling of $a = 31$ mT$/\mu_B$ and the Kondo temperature $T_K = 1.3$ K. The low-temperature plateau in K corresponds to a strongly reduced average impurity magnetic moment, $M = KB/a = 0.017\mu_B$ at $B = 0.3$ T, due to Kondo screening. **b**, The field dependence of the experimental Knight shift (symbols) deep in the strong-Kondo coupling regime and the NRG theoretical prediction (line).

accessible temperatures [20], three orders of magnitude below the dominant exchange interactions [21]. As revealed in our recent muon spin rotation and relaxation (μSR) study [22], the corresponding spinon excitations are gapless and form a spinon Fermi surface. This investigation has further disclosed that impurities, originating from intrinsic 6–9% Cu–Zn intersite disorder [2], are strongly magnetically coupled to the spin liquid and that their magnetic behaviour is characterized by a low-temperature magnetization plateau with a strongly reduced magnetic moment. This could be a sign of Kondo physics.

In-depth μSR experiments on Zn-brochantite that are reported here indeed confirm the first realization of the Kondo effect in a charge insulator (Fig. 1). The impurity magnetization extracted from the muon Knight shift clearly demonstrates the crossover from the weak-Kondo-coupling regime at high temperatures to the strong-Kondo-coupling regime at low temperatures. Furthermore, magnetic-field-induced changes at the Fermi level characteristic of the Kondo effect are detected through muon spin relaxation. These experimental findings are supported by numerical renormalization group (NRG) calculations, which furthermore show that the Kondo screening might be affected by spinon–spinon interactions mediated by emergent gauge fields.

First, we prove that impurities in Zn-brochantite are not free. To show this, we use muons, which represent ideal local probes of impurity magnetism. They are dominantly coupled to impurity spins at low temperatures, as demonstrated by a linear scaling of the muon-detected local susceptibility with impurity susceptibility [22], yield-

ing a magnetic coupling of $a = 31$ mT$/\mu_B$ between the muon spin and the surrounding impurities (see Methods). The muon Knight shift K (see Methods), which is proportional to the local impurity magnetization M normalized by the applied magnetic field B, $K = aM/B$ [23] increases monotonically with decreasing temperature (Fig. 2a). In the applied field of 0.3 T it reaches a plateau value of 0.18% at the lowest temperatures . This yields an average magnetic moment of $M = KB/a = 0.017\mu_B$ per magnetic Cu^{2+} ion. As the spin-1/2 impurity concentration in Zn-brochantite is estimated at 6–9% [2], the average magnetic moment per impurity is in the range of 0.19–0.28 μ_B. This is significantly short of the full value of 1.0–1.2 μ_B expected for the Cu^{2+} ions, the value that would be observed for low-temperature saturation of free impurity spins in an applied magnetic field. Furthermore, the low-temperature Knight-shift saturation plateau gets reduced by only a factor of ~1.4 in a more than three-times larger field of 0.93 T (Fig. 2a), not by the factor $0.93/0.3 = 3.1$ that would apply to free impurities.

As an alternative to free impurities, one should consider an interpretation based on impurity–impurity coupling. A reduction of the average impurity magnetic moment could naturally result from the formation of spin singlets in even-sized clusters of, e.g., antiferromagnetically coupled impurities. However, to reproduce the experimental reduction of the average impurity moment, a large majority of impurities would have to be clustered, which is not compatible with their moderate concentration of 6–9% (see Supplementary Fig. 1) assuming couplings only between nearest-neighbour randomly-positioned impurities (see Supplementary Information).

If longer-range couplings between impurities are present — either due to random far-neighbour exchange couplings, long-range dipolar couplings, or effective RKKY couplings mediated by the spinon Fermi sea — a random-singlet phase should form [24] due to random distribution of impurities across the material. If this were the case, a random-coupling spin-glass type of behaviour would be expected at the lowest temperatures [24], which, however, contradicts the experimental results in several significant ways. Specifically, in Zn-brochantite the temperature dependence of the magnetization (Fig. 2a), the specific heat [2] and the muon-spin-relaxation rate [21] are all smooth and do not feature any kink-like maxima characteristic of spin glasses [25].

As the reduction of the impurity magnetization cannot be explained in an impurity-only picture, we next turn to the scenario of impurities coupled to the spin-liquid state. Namely, we consider the Kondo effect, where the impurity spin gets screened by spinful itinerant quasiparticles [2]. In this case, the crossover between the high-temperature weak-coupling regime and the low-temperature strong-coupling regime is predicted to yield a smooth rise of impurity magnetization. Furthermore, a magnetization plateau corresponding to reduced impurity magnetic moment is expected at low temperatures [26]. This is precisely what is observed in Zn-brochantite (Fig. 2a). In order to quantitatively compare our experiment with the predicted Kondo impurity magnetization, we have performed NRG calculations within the framework of a non-interacting Fermi liquid (see Methods), as this method has proven indispensable in describing the Kondo effect in a fully general setting [2, 27]. Taking into account the impurity g factor $g = 2.3$ (see below) and the magnetic coupling a, we achieve a good agreement between the experimental data and NRG predictions for both fields at all temperatures (Fig. 2a). In this calculation, there were only two free fitting parameters: the impurity concentration and the Kondo temperature. The former turns out to be $p = 11(2)\%$, which is consistent with the 6–9% concentration estimate from various bulk measurements [2]. For the Kondo temperature, on the other hand, we get $T_K = 1.3(1)$ K, which is almost the same as the impurity Curie-Weiss temperature $|\theta| = 1.2$ K determined from bulk susceptibility above ∼1 K [2]. This is in agreement with Kondo theory, which predicts a Curie-Weiss-like dependence of the impurity magnetization with $|\theta| \simeq T_K$ above T_K [2].

A definitive proof of the spinon-based Kondo screening in Zn-brochantite is the observation of Kondo-resonance splitting (Fig. 3), a hallmark of the Kondo effect that is well known from the standard description of the strongly-coupled Kondo regime [2, 28]. The Kondo resonance is a characteristic enhancement of the local density of states (DOS) around the Fermi level associated with the coupling between the impurity spin and the itinerant host

quasiparticles. Its width at zero temperature is given by the Kondo temperature and increases with increasing temperature [28] due to thermal excitations. Kondo-resonance splitting occurs above a finite critical magnetic field $B^*(T)$, when the field perturbs the resonance to such a degree that the splitting of its spin-up and spin-down components becomes larger than the zero-field resonance width. Consequently, the DOS at the Fermi level gets decreased above B^*. The muon spin relaxation rate λ should also decrease above the same field. This is because λ probes local-magnetic-field fluctuations [23] and thus couples to magnetic excitations at the Fermi level in a spinon metal, in close resemblance to nuclear magnetic resonance (NMR) spin-lattice relaxation rate in a standard metal, which is proportional to the squared DOS at the Fermi level [4]. Indeed, we have already reported an anomalous reduction of the muon spin relaxation rate λ above $B^* \sim 0.4$ T [22]. However, as those data were limited to a single temperature of 110 mK, only a conjecture of a possible field-induced instability of the spin liquid could be made at that time.

Our new, more comprehensive field-dependent muon spin relaxation-rate data collected at various temperatures below T_K (Fig. 3) demonstrate instead that the anomaly at B^* is a manifestation of the Kondo resonance splitting. We find that the anomaly field B^* scales linearly with temperature, $B^* = B_0^* + \frac{k_B T}{g\mu_B}$, where k_B and μ_B are the Boltzman constant and the Bohr magneton, respectively, and $B_0^* = 0.36(6)$ T is the extrapolated zero-temperature anomaly field. The extracted g factor $g = 2.3(3)$ is the same as the value $g \sim 2.2$ found in the low-temperature Schottky impurity contribution to specific heat [2] and is typical for the Cu^{2+} moments in an oxygen crystal-field environment. Importantly, this g factor is an order of magnitude larger than the effective g factor that corresponds to an NMR-observed intrinsic field-induced instability of the spinon-metal state in Zn-brochantite below a field-dependent critical temperature T_c (Fig. 1) due to spinon pairing [18]. Therefore, the muon-detected anomaly at B^* is not related to the latter instability. On the other hand, in the Kondo picture, Kondo resonance splitting should occur at zero temperature at the field of the order of magnitude given by $\frac{k_B T_K}{g\mu_B} = 0.8$ T [28, 30], which agrees reasonably well with experiment. The fact that B_0^* is finite is a distinctive feature of the Kondo effect. Furthermore, B^* is predicted to increase linearly with temperature due to an increasing width of the Kondo resonance [28], again in agreement with experiment (Fig. 3f). Finally, we note that the power-law dependence $\lambda \propto B^{-\eta}$ changes at B^* from being rather weak ($\eta = 0.23(3)$) at $B < B^*$ to being much stronger ($\eta = 2.4(3)$) at $B > B^*$ (Fig. 3a-e). The high-field power is close to 2, the value characteristic of a single-exponential time decay of the local-field autocorrelation function [23] that is consistent with effectively quasi-free impurities above the Kondo resonance split-
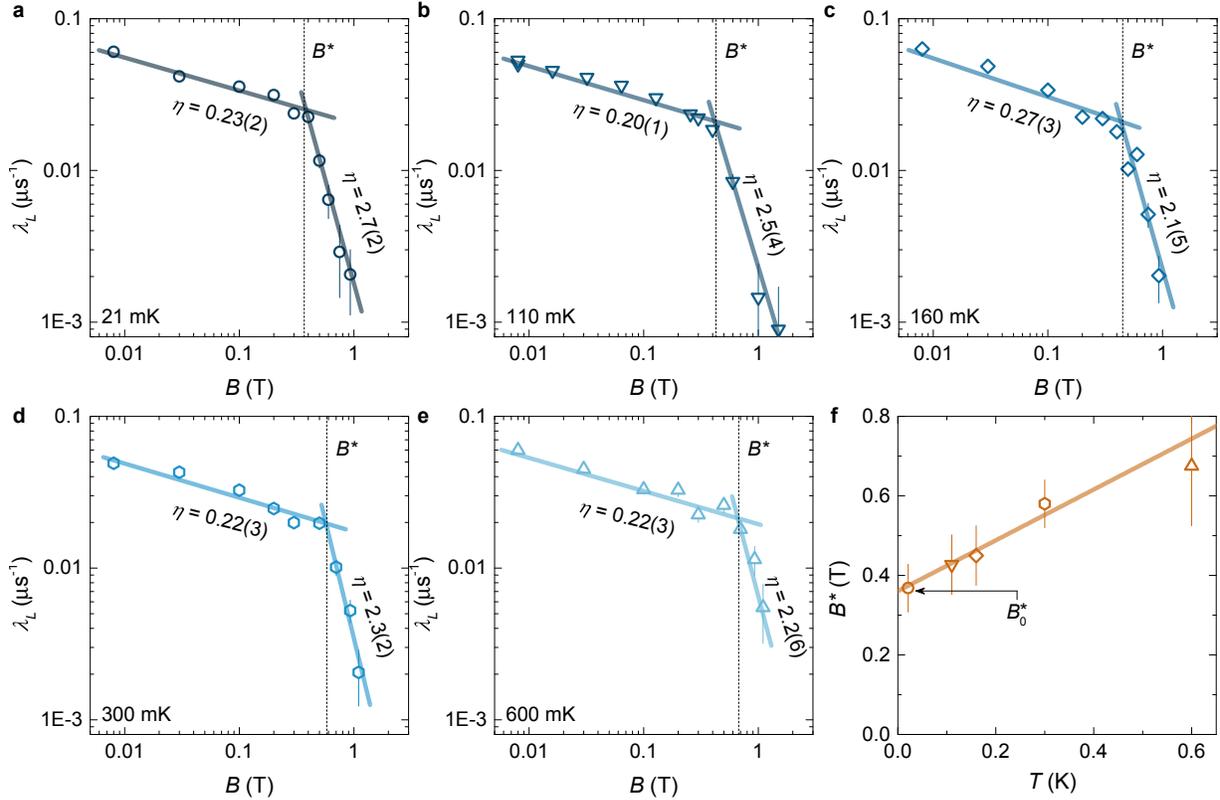
Dynamical μSR signature of the Kondo effect. a-e, The field dependence of the muon spin relaxation rate λ at various temperatures in the strong-Kondo-coupling regime (symbols). Solid lines correspond to the power law $\lambda \propto B^{-\eta}$, while the dashed vertical lines indicate the anomaly field B^*, where $\lambda(B)$ changes its power-law dependence. This field corresponds to the Kondo-resonance splitting, a hallmark of the Kondo effect. **f**, The temperature dependence of the anomaly field B^* (symbols). The line demonstrates the linear scaling $B^* = B_0^* + k_B T/(g\mu_B)$, with the zero-temperature anomaly field $B_0^* = 0.36(6)$ T and g factor $g = 2.3(3)$.

ting field. The low-field power $\eta = 0.23(3)$, on the other hand, is close to 0, the value expected for a spinful impurity in a metal in the low-field strong-Kondo-coupling regime [2].

The power-law muon relaxation $\lambda \propto B^{-0.2}$ (Fig. 3a-e) at low fields instead of the expected field independence and the apparently systematically faster decrease of the impurity magnetization with increasing magnetic field than the simplest non-interacting Kondo theory predicts for the strong-Kondo-coupling regime (Fig. 2b) are signs of a modified Kondo response in Zn-brochantite that can be due to spinon–spinon interactions. From the theoretical point of view, it was predicted by Ribeiro and Lee [15] that in a spin-1/2 U(1) spinon metal the local susceptibility at the impurity site is insensitive to gauge degrees of freedom, which mediate the spinon–spinon interactions. However, this conjecture is based on retaining only the leading order in a large-N expansion, which, in the case of the U(1) spinon metal, corresponds to a random-phase approximation. Therefore higher-order corrections could lead to deviations brought about by spin-liquid gauge fields [15].

We find that the experimentally implied disagreements with the generic Kondo impurity response are indeed most likely to originate from emergent gauge fields. These deviations could, *a priori*, be due to various perturbations to the conventional Kondo model of a rotationally-symmetric spin-1/2 magnetic impurity coupled to a bath of spinful non-interacting fermions with a constant density of states. The perturbations of interest are those that break the full Kondo universality. We have tested several of them by more elaborate NRG calculations of the impurity magnetization, as detailed in Methods. We find that neither a finite spinon bandwidth, a finite g factor of the spinons, a non-constant spinon DOS, an anisotropy of the Kondo coupling, nor a partial gap opening in the spinon DOS in an applied magnetic field can account for the experimental results (Supplementary Fig. 2). Moreover, even a finite impurity concentration leading to a dilute Kondo lattice with coupling between the impurity spins cannot be responsible for the observed response (Supplementary Fig. 3). The only plausible explanation of the possibly systematic discrepancy between the muon Knight shift at low tem-

peratures and the Kondo theory that we can envisage is therefore based on non-negligible spinon–spinon interactions mediated through emergent spin-liquid gauge fields. As regards this experimental observation, the gauge fields phenomenologically manifest in an effective renormalization of the relevant g factors (Supplementary Fig. 4), whatever their microscopic effect may be. The importance of gauge-field fluctuations in Zn-brochantite is also directly reflected in the intrinsic spinon-pairing instability of the spinon-metal state, as well as in a power-law dependence of the NMR relaxation rate $1/T_1 \propto T^{0.8}$ in the spinon-metal regime [18], instead of the Korringa relation $1/T_1 \propto T$ that holds for non-interacting fermions [4]. It is expected that gauge-field fluctuations should introduce corrections to dynamical spin correlation functions with a power-law dependence [31, 32]. However, more rigorous predictions are needed to accurately assess the importance of gauge fields in the spinon-based Kondo effect, even though such calculations for interacting itinerant particles currently represent a huge theoretical challenge.

As the predicted Kondo response greatly depends on the exact nature of the host spin liquid [13], Kondo-coupled impurities could, firstly, be utilized to study spinon excitations and the corresponding gauge fields in this enigmatic state of matter. This is a promising alternative to direct experimental studies in local observables, which are very challenging [33–36], because spin liquids lack symmetry-breaking order and their spinon excitations carry no charge, making them notoriously difficult to detect. A further advantage is that the impurity response to the external field is usually much larger than the intrinsic spin-liquid response, which is dominated by singlets. Secondly, certain spin liquids feature topologically-protected quasiparticles, e.g., non-Abelian anyons [36, 37], which, in principle, makes them promising candidates for robust quantum computing [37]. However, finding a way of manipulating these states in a solid-state device is a key outstanding issue. The required level of control could potentially be achieved by exploiting the Kondo coupling, by manipulating impurities to achieve the desired change in the spin liquid. One concrete theoretical proposal in this spirit is based on the Kitaev honeycomb spin-liquid, where the weak- and strong-Kondo-coupling limits are predicted to correspond to different topologies of the spin-liquid ground state [16].

---

* andrej.zorko@ijs.si

[1] Kondo, J. Resistance minimum in dilute magnetic alloys. *Prog. Theor. Phys.* **32**, 37–49 (1964).

[2] Hewson, A. C. *The Kondo Problem to Heavy Fermions* (Cambridge University Press, Cambridge, 1997).

[3] Goldhaber-Gordon, D. *et al.* Kondo effect in a single-electron transistor. *Nature* **391**, 156–159 (1998).

[4] Cronenwett, S. M., Oosterkamp, T. H. & Kouwenhoven, L. P. A tunable Kondo effect in quantum dots. *Science* **281**, 540–544 (1998).

[5] Nygård, J., Cobden, D. H. & Lindelof, P. E. Kondo physics in carbon nanotubes. *Nature* **408**, 342–346 (2000).

[6] Park, J. *et al.* Coulomb blockade and the Kondo effect in single-atom transistors. *Nature* **417**, 722–725 (2002).

[7] Yu, L. H. & Natelson, D. The Kondo effect in C_{60} single-molecule transistors. *Nano Lett.* **4**, 79–83 (2004).

[8] Cronenwett, S. M. *et al.* Low-temperature fate of the 0.7 structure in a point contact: A Kondo-like correlated state in an open system. *Phys. Rev. Lett.* **88**, 226805 (2002).

[9] Iqbal, M. J. *et al.* Odd and even Kondo effects from emergent localization in quantum point contacts. *Nature* **501**, 79–83 (2013).

[10] Chen, J.-H., Li, L., Cullen, W. G., Williams, E. D. & Fuhrer, M. S. Tunable Kondo effect in graphene with defects. *Nat. Phys.* **7**, 535–538 (2011).

[11] Khaliullin, G. & Fulde, P. Magnetic impurity in a system of correlated electrons. *Phys. Rev. B* **52**, 9514–9519 (1995).

[12] Sushkov, O. P. Spin-1/2 magnetic impurity in a two-dimensional magnetic system close to a quantum critical point. *Phys. Rev. B* **62**, 12135–12140 (2000).

[13] Kolezhuk, A., Sachdev, S., Biswas, R. R. & Chen, P. Theory of quantum impurities in spin liquids. *Phys. Rev. B* **74**, 165114 (2006).

[14] Florens, S., Fritz, L. & Vojta, M. Kondo effect in bosonic spin liquids. *Phys. Rev. Lett.* **96**, 036601 (2006).

[15] Ribeiro, P. & Lee, P. A. Magnetic impurity in a $U(1)$ spin liquid with a spinon Fermi surface. *Phys, Rev. B* **83**, 235119 (2011).

[16] Dhochak, K., Shankar, R. & Tripathi, V. Magnetic impurities in the honeycomb Kitaev model. *Phys. Rev. Lett.* **105**, 117201 (2010).

[17] Vojta, M., Mitchell, A. K. & Zschocke, F. Kondo impurities in the Kitaev spin liquid: Numerical renormalization group solution and gauge-flux-driven screening. *Phys. Rev. Lett.* **117**, 037202 (2016).

[18] Gomilšek, M. *et al.* Field-induced instability of a gapless spin liquid with a spinon Fermi surface. *Phys. Rev. Lett.* **119**, 137205 (2017).

[19] Li, Y. *et al.* Gapless quantum spin liquid in the $S = 1/2$ anisotropic kagome antiferromagnet $ZnCu_3(OH)_6SO_4$. *New J. Phys.* **16**, 093011 (2014).

[20] Norman, M. R. Colloquium: Herbertsmithite and the search for the quantum spin liquid. *Rev. Mod. Phys.* **88**, 041002 (2016).

[21] Gomilšek, M. *et al.* Instabilities of spin-liquid states in a quantum kagome antiferromagnet. *Phys. Rev. B* **93**, 060405(R) (2016).

[22] Gomilšek, M. *et al.* μSR insight into the impurity problem in quantum kagome antiferromagnets. *Phys. Rev. B* **94**, 024438 (2016).

[23] Yaouanc, A. & De Réotier, P. D. *Muon Spin Rotation, Relaxation, and Resonance: Spplications to Condensed Matter* (Oxford University Press, Oxford, 2011).

[24] Kimchi, I., Nahum, A. & Senthil, T. Valence bonds in random quantum magnets: Theory and application to YbMgGaO$_4$. *Phys. Rev. X* **8**, 031028 (2018).

[25] Mydosh, J. A. Spin glasses: redux: an updated experimental/materials survey. *Rep. Prog. Phys.* **78**, 052501 (2015).

[26] Žitko, R. Magnetization curves for anisotropic magnetic impurities adsorbed on a normal metal substrate. In Bonča, J. (ed.) *Physical Properties of Nanosystems*, 247–257 (Springer, 2011).

[27] Wilson, K. G. The renormalization group: Critical phenomena and the Kondo problem. *Rev. Mod. Phys.* **47**, 773–840 (1975).

[28] Costi, T. A. Kondo effect in a magnetic field and the magnetoresistivity of Kondo alloys. *Phy. Rev. Lett.* **85**, 1504–1507 (2000).

[29] Abragam, A. *The Principles of Nuclear Magnetism* (Oxford University Press, Oxford, 1961).

[30] Kretinin, A. V. *et al.* Spin-1/2 Kondo effect in an InAs nanowire quantum dot: Unitary limit, conductance scaling, and Zeeman splitting. *Phys. Rev. B* **84**, 245316 (2011).

[31] Itou, T., Oyamada, A., Maegawa, S. & Kato, R. Instability of a quantum spin liquid in an organic triangular-lattice antiferromagnet. *Nat. Phys.* **6**, 673–676 (2010).

[32] Metlitski, M. A., Mross, D. F., Sachdev, S. & Senthil, T. Cooper pairing in non-Fermi liquids. *Phys. Rev. B* **91**, 115111 (2015).

[33] Han, T.-H. *et al.* Fractionalized excitations in the spin-liquid state of a kagome-lattice antiferromagnet. *Nature* **492**, 406–410 (2012).

[34] Paddison, J. A. M *et al.* Continuous excitations of the triangular-lattice quantum spin liquid YbMgGaO$_4$. *Nat. Phys.* **13**, 117–122 (2017).

[35] Klanjšek, M. *et al.* A high-temperature quantum spin liquid with polaron spins. *Nat. Phys.* **13**, 1130–1134 (2017).

[36] Janša, N. *et al.* Observation of two types of fractional excitation in the Kitaev honeycomb magnet. *Nat. Phys.* **14**, 786–790 (2018).

[37] Kitaev, A. Y. Fault-tolerant quantum computation by anyons. *Ann. Phys.* **303**, 2–30 (2003).

AUTHOR CONTRIBUTIONS

A.Z. conceived, designed and supervised the project. M.G. and A.Z. performed the μSR measurements, with technical assistance of C.B., and analysed the data. R.Ž. carried out the NRG calculations. M.G. developed the percolation-theory-based model for impurity-cluster spin. Y.L. and Q.M.Z. synthesized and characterized the sample. All authors discussed the results. A.Z. wrote the paper with feedback from all authors.

COMPETING INTERESTS

The authors declare no competing interests.

ADDITIONAL INFORMATION

Supplementary information is available for this paper.

Correspondence and requests for materials should be addressed to A.Z.

METHODS

μSR measurements

The μSR investigation was conducted on the LTF instrument at the Paul Scherrer Institute (PSI), Switzerland, on a $\sim$100% deuterated powder sample from the same batch as the one used in our previous investigations [18, 21, 22]. The sample was glued onto a silver sample holder with diluted GE Varnish to ensure good thermal conductivity. The measurements were performed between 21 mK and 10 K in various transverse (TF) and longitudinal (LF) applied fields $B \leqslant 1$ T with respect to the initial muon-spin polarization.

In the TF setup the initial muon polarization was tilted by $\sim$45$°$ away from the beam/field direction. Its component perpendicular to the field was detected by a set of detectors. The muon asymmetry $A(t)$, which is proportional to the muon polarization [23], was measured and modelled by

$$
\begin{aligned}
A_{TF}(t) &= A_1 \cos\left(2\pi\nu_1 t + \phi\right) e^{-\lambda_1 t} \\
&+ A_2 \cos\left(2\pi\nu_2 t + \phi\right) e^{-\lambda_2 t},
\end{aligned} \quad (1)
$$

where the total initial muon asymmetry was $A_1 + A_2 = 0.199(12)$ and the ratio of the two components was $A_2/A_1 = 22\%$. A typical TF muon asymmetry curve is shown in the Supplementary Fig. 5 together with the corresponding Fourier transform. The fitting parameters are given in the Supplementary Methods. The signal A_1 was attributed to the muons stopping in the sample and the signal A_2 to the muons stopping in the diamagnetic silver sample holder. Since the background was diamagnetic, it decayed in time much more slowly than the intrinsic signal ($\lambda_2 \ll \lambda_1$) and its temperature-independent oscillation frequency ν_2 could be used as the reference Larmor frequency. The Knight shift was calculated as

$$
K = (\nu_1 - \nu_2)/\nu_2. \quad (2)
$$

Combining the new μSR measurements with those previously published in Ref. 22 we could better constrain the *a priori* unknown backgrounds in both experiments by comparing and simultaneously fitting old and new measurements at the same values of T and B. After a careful self-consistent fit of all measured data, we found that the best estimates of low-field Knight-shift values were reduced by $\sim$15% in relative terms when compared to the data published in Ref. 22. Consequently, the magnetic coupling between the muon spin and the impurities, $a = 31$ mT/μ_B, is reduced by the same amount compared to the previously published value. The new values should be taken as the definitive ones.

In the LF setup, which was used to measure the longitudinal muon relaxation rate λ, the initial muon-spin polarization was along the beam/field direction and the muon asymmetry was measured along the same direction. The asymmetry was modelled with a stretched-exponential model

$$
A_{LF}(t) = A_1 e^{-(\lambda t)^\beta} + A_2, \quad (3)
$$

where the total initial asymmetry was $A_1 + A_2 = 0.239(4)$, with the same ratio $A_2/A_1 = 22\%$ as in the TF experiment. The same stretching exponent $\beta = 0.86(5)$ was found as in our previous LF studies [21, 22]. A typical set of LF muon asymmetry curves at a selected temperature is shown in the Supplementary Fig. 5c.

NRG calculations

The numerical renormalization group (NRG) method [27, 39] was utilized to compute the impurity magnetization as a function of magnetic field and temperature. We used the discretisation parameter $\Lambda = 2$, averaged over two discretisation grids, and kept a high number of states to ensure full convergence. The Wilson's thermodynamic definition [27] of the Kondo temperature where $T_K \chi_{\text{imp}}(T_K) = 0.07$ was applied. Here χ_{imp} is the impurity contribution to the total-system's magnetic susceptibility. The reference calculations were performed for a spin-1/2 magnetic impurity with an isotropic Kondo exchange coupling to a bath of non-interacting spin-1/2 fermions with a constant density of states in a wide-band limit.

The Hamiltonian of the reference model is

$$
H = \sum_{k\sigma} \epsilon_k c_{k\sigma}^\dagger c_{k\sigma} + J\mathbf{S} \cdot \mathbf{s}(\mathbf{r} = 0) + g\mu_B S_z B \quad (4)
$$

where the operators $c_{k\sigma}$ describe itinerant particles with momentum k, spin σ, and energy ϵ_k, J is the Kondo exchange coupling, $\mathbf{S}$ is the quantum-mechanical spin-1/2 operator of the impurity, $\mathbf{s}(\mathbf{r} = 0)$ is the spin density of the itinerant particles at the position of the impurity, g is the impurity g-factor, μ_B the Bohr magneton, and B the magnetic field. T_K is given approximately by $T_K = D\sqrt{\rho J} \exp(-1/\rho J)$. Here D is the half-bandwidth of the itinerant-particles band and $\rho = 1/(2D)$ is the corresponding density of states.

The reference model describes the intermediate and high temperature ranges very well (Fig. 2a). At low temperatures we find a deviation, which is still within the experimental uncertainty (and hence perhaps not even statistically significant), but quite systematic. The slope of the calculated $M(B)/B$ curve is appreciably smaller than the slope of the measured $K(B)$ data points at 21 mK (Fig. 2b). Therefore, additional sets of calculations were performed for various perturbations.

Finite spinon bandwidth: We first relaxed the assumption of the wide-band limit $T_K \ll D$, where D is the half-bandwidth of the conduction band. We considered the Kondo impurity model with a flat band with

$\rho J = 0.7$ and $T_K/D \approx 0.5$, while the reference model had $\rho J = 0.15$ and $T_K/D = 4.2 \times 10^{-4}$. For this rather extreme case, the agreement with experiment is slightly improved at low temperatures, but is worse at high temperatures (Supplementary Fig. 2a).

Finite spinon g factor: In the wide-band limit, the Zeeman term of the itinerant particles can be neglected, since the impurity magnetic susceptibility $\chi_i \propto 1/T_K$ is much larger than the Pauli susceptibility of the band, $\chi_b \propto 1/D$. The case of a finite Zeeman term in the conduction band, which was included in the calculation as described in Ref. 40, with the spinon g factor equal to the impurity g factor was therefore considered for a still rather narrow band so that $T_K/D \approx 0.2$ (by taking $\rho J = 0.5$). The Hamiltonian thus had an additional term $H' = g_b \mu_B B \sum_k (1/2)(c_{k\uparrow}^\dagger c_{k\uparrow} - c_{k\downarrow}^\dagger c_{k\downarrow})$. For this model, the slope of M/B vs. B at low temperatures is actually reduced compared to the reference model (Supplementary Fig. 2b).

Non-constant spinon DOS: Since in a narrow-band situation the details of DOS in the continuum, $\rho(\epsilon)$, may play a larger role, we investigated some possible modifications for $\rho(0)J = 0.5$, e.g. a large slope of DOS ρ across the Fermi level. This was found to have little effect on the results. In Supplementary Fig. 2c we show the case of a triangular-shaped DOS with $\rho(\epsilon) = \rho(0)(D - \epsilon)/D$ for a narrow-band calculation with $T_K/D \approx 0.2$. Furthermore, potential scattering on the impurity site, a perturbation of the form $H' = V n(\mathbf{r} = 0)$ where V is the local potential and $n(\mathbf{r})$ the density of itinerant quasiparticles at the position of the impurity, was also found to play little role (Supplementary Fig. 2d). Only strong singularities in ρ close to the Fermi level could potentially lead to significant effects.

Kondo-coupling anisotropy: The Kondo exchange coupling term of the Hamiltonian can be separated into the transverse and longitudinal parts, $H_K = J_\perp(S_x s_x + S_y s_y) + J_\parallel S_z s_z$. We studied both the limit of a dominant Ising Kondo exchange coupling ($\rho J_\parallel = 1.5$ and $\rho J_\perp = 0.075$, so that $J_\parallel/J_\perp = 20$) and a dominant transverse coupling ($\rho J_\parallel = 0.05$ and $\rho J_\perp = 0.5$, so that $J_\parallel/J_\perp = 0.1$), yielding a comparable Kondo temperature $T_K/D \approx 0.04$. Even for these unphysically large anisotropy ratios only small changes of M/B curves were found (Supplementary Fig. 2e). This can be explained by the fact that the renormalization group flow toward the strong-coupling fixed point for the anisotropic Kondo model tends to restore the isotropy at low energy scales [2].

Partial gap opening in the spinon DOS: At low temperatures and sizeable fields the quantum spin liquid in Zn-brochantite becomes partially gapped through a field-induced spinon-pairing instability [18]. The fraction of residual ungapped spinons is $f = 0.3$ at $B = 1$ T and decreases with increasing field. The behaviour for $B < 1$ T is not known, therefore a linear extrapolation to low fields

with $f = 1$ at $B = 0$ was made. As the simplest approximation to incorporate the partial gap opening in the calculations we assumed a modification of the conduction-band DOS proportional to the gapped fraction $1 - f$ of spinons. For this gapped fraction we considered the case of a hard gap of width Δ, and the case of a BCS-like redistribution of the spectral weight with $\Delta_{\mathrm{BCS}} = \Delta$. The partial gapping of spinons leads to reduced Kondo screening at very low temperatures due to a decreased spinon DOS at the Fermi level, hence the impurity magnetization is enhanced at low temperatures (Supplementary Fig. 2f). This effect increases in strength as the magnetic field is increased, thus inverting the slope of the $K(B)$ curve at low temperatures, which clearly contradicts the experiment. We note that extreme versions of the DOS reduction were assumed with a full suppression in the energy range $|\epsilon| < \Delta$. The actual gap is very likely to be softer.

Finite impurity concentration: The impurity concentration of 6–9% in Zn-brochantite [2] is sufficiently large to prompt the question of possible impurity–impurity-coupling corrections to the dilute-limit results. The relevant model to describe this situation is the Kondo lattice model (KLM) with a random distribution of spins. The corresponding Hamiltonian consists of a tight-binding lattice of non-interacting itinerant fermions with density n ($n = 1$ is a half-filled band) and additional local moments ($S = 1/2$ spins) coupled by the Kondo exchange coupling on a random subset of sites with concentration p. We calculated $M(B,T)$ using the real-space dynamical mean-field theory (RDMFT) with the NRG as the impurity solver. This is a conceptually simple (but numerically expensive) way to extend the single-impurity NRG results to the case of a finite impurity concentration. The calculations were performed on a 17×17 lattice with electron occupancy $n = 0.5$ (quarter-filled band), for $\rho J = 0.4$. For low impurity concentrations the curves are all very similar – the curves for $p = 1\%$ and $p = 10\%$ actually overlap within the numerical errors (Supplementary Fig. 3). At $p = 20\%$, some deviations are observable in the high-field range, while the low-field results are still little affected. We thus conclude that the 6–9% impurity concentration in Zn-brochantite can be safely considered as corresponding to the "dilute limit" where the magnetization can be computed using the single-impurity model. This is also in line with heavy-fermion systems where the magnetic susceptibility and other quantities scale with the concentration of magnetic ions over a surprisingly large concentration range [41]. A magnetization plateau that is found in the dense-impurity limit at intermediate fields (Supplementary Fig. 3) is consistent with theory [42, 43] and corresponds to a transition from a paramagnetic state to a ferromagnetic half-metal state, indicating the existence of a well-defined partial gap.

Renormalization of g factors: Finally, we mention two cases that lead to theoretical predictions in better agree-

ment with experiment, but do so for parameter values that either differ from the experimentally established ones or are clearly unphysical. An example of the former case is the assumption of the impurity g factor much in excess of $g = 2.3$. In Supplementary Fig. 4a we show the calculation with $g = 6.5$, which are in near-perfect agreement with experiment at all temperatures and fields. An example of the latter case is the assumption of a large negative value for the g factor of the itinerant fermions. In Supplementary Fig. 4b we show the calculations for $g_b = -3$, which fit the low temperature results almost perfectly, but, however, deviate from experiment at high temperatures.

DATA AVAILABILITY

The data that support the findings of this study are available from the corresponding author upon reasonable request.

————————

* andrej.zorko@ijs.si

[38] Suter, A., Mali, M., Roos, J. & Brinkmann, D. Mixed magnetic and quadrupolar relaxation in the presence of a dominant static Zeeman Hamiltonian. *J. Phys.: Condens. Matter* **10**, 5977–5994 (1998).

[39] Žitko, R. & Pruschke, T. Energy resolution and discretization artefacts in the numerical renormalization group. *Phys. Rev. B* **79**, 085106 (2009).

[40] Höck, M. & Schnack, J. Numerical renormalization group calculations of the magnetization of Kondo impurities with and without uniaxial anisotropy. *Phys. Rev. B* **87**, 184408 (2013).

[41] Lin, C. L., Wallash, A., Crow, J. E., Mihalisin, T. & Schlottmann, P. Heavy-fermion behavior and the single-ion Kondo model. *Phys. Rev. Lett.* **58**, 1232–1235 (1987).

[42] Kusminskiy, V. S., Beach, A., K. Castro Neto & Campbell, D. Mean-field study of the heavy-fermion metamagnetic transition. *Phys. Rev. B* **77**, 094419 (2008).

[43] Golež, D. & Žitko, R. Lifshitz phase transitions in the ferromagnetic regime of the Kondo lattice model. *Phys. Rev. B* **88**, 054431 (2013).

Supplementary information:
Kondo screening in a charge-insulating spinon metal

M. Gomilšek,[1,2] R. Žitko,[1,3] M. Klanjšek,[1] M. Pregelj,[1] C. Baines,[4] Y. Li,[5] Q. M. Zhang,[6,7] and A. Zorko[1,*]

[1] *Jožef Stefan Institute, Jamova c. 39, SI-1000 Ljubljana, Slovenia*
[2] *Centre for Materials Physics, Durham University, South Road, Durham, DH1 3LE, UK*
[3] *Faculty of Mathematics and Physics, University of Ljubljana, Jadranska c. 19, SI-1000 Ljubljana, Slovenia*
[4] *Laboratory for Muon Spin Spectroscopy, Paul Scherrer Institute, CH-5232 Villigen PSI, Switzerland*
[5] *Experimental Physics VI, Center for Electronic Correlations and Magnetism,*
University of Augsburg, 86159 Augsburg, Germany
[6] *National Laboratory for Condensed Matter Physics and Institute of Physics,*
Chinese Academy of Sciences, Beijing 100190, China
[7] *School of Physical Science and Technology, Lanzhou University, Lanzhou 730000, China*

SUPPLEMENTARY NOTES

Clustering of Impurities

In this section we demonstrate that any spin model with only short-range two-spin couplings between randomly-placed impurities obeys a stringent lower bound on the average value of the spin per impurity. This exact lower bound depends only on the topology of the possible couplings, and not on the precise type or strength of these couplings, and is a simple consequence of the rules for quantum addition of spin. Furthermore, we show that this bound is experimentally violated in Zn-brochantite, refuting such a simple scenario of impurity magnetism in this system.

Exact lower bound on average impurity spin

Assuming that possible impurity sites are occupied uniformly randomly with probability (impurity concentration) p, the impurities will, by pure chance, form coupled impurity clusters of various sizes. Due to quantum spin addition rules, even-sized impurity clusters can, in principle, have total spin zero (forming singlets), but odd-sized clusters of spin-$1/2$ impurities must retain a total spin of at least $1/2$, a reduction by a factor of $1/s$, where s is the (odd) cluster size, compared to the case of s uncoupled impurities where the maximal spin is $s/2$. Coupled clusters of odd size s (including lone, free impurities as $s = 1$ clusters) can thus only reduce the average spin per constituent impurity by a factor of $1/s$, regardless of the type of coupling. A lower bound on the spin reduction factor $f(p) = \langle S \rangle /S$, by which the average spin per impurity $\langle S \rangle$ can be reduced from its full value of $S = 1/2$ by impurity–impurity couplings, is then given

for the whole impurity lattice by

$$f(p) \geq m(p) = \sum_{s \text{ odd}} \frac{w_s(p)}{s} \qquad (1)$$

where $w_s(p) \geq 0$ is the probability that a randomly-selected impurity is part of a cluster of size s.

The cluster-size probabilities $w_s(p)$ are studied in uncorrelated site percolation theory [1] and depend only on the topological connectivity of the underlying lattice of impurity sites. Two impurity sites are considered connected (adjacent) when they would have a non-zero impurity–impurity coupling if they were both actually occupied by an impurity. Note that the probabilities $w_s(p)$ do not depend on the specific type or strength of the impurity-impurity couplings, just on their spatial distribution and the distance range over which these couplings connect the impurities.

The first term, $w_1(p)$, in $m(p) \geq w_1(p)$ describes the contribution of lone impurities with no occupied adjacent impurity sites, which s behave are thus just free spins and contribute fully to the total impurity moment. The fraction of lone impurities is given by $w_1(p) = (1 - p)^z$ and depends only on the coordination number z (the number of sites adjacent to a given site) of the impurity-site lattice, assuming that z is the same for all impurity sites.

Generalizing Eq. (1) to impurities with arbitrary bare spin $S \geq 1/2$, we find that the lower bound on the spin reduction factor $f(p) = \langle S \rangle /S$ is given by

$$f(p) \geq m_S(p) = \alpha_S \cdot m(p) + (1 - \alpha_S) \cdot w_1(p) \qquad (2)$$

where $m(p)$ is defined by Eq. (1), and where $\alpha_S = 1/(2S)$ for half-integer S while $\alpha_S = 0$ for integer S (giving $m_S \equiv w_1$). This difference in α_S is due to the fact that odd-sized clusters of size $s \geq 3$ must have a spin of at least $1/2$ for half-integer S, while they can form spin-zero singlets for integer S. On the other hand, even clusters can always, in principle, form spin singlets, while lone ($s = 1$) impurities always carry full spin S.
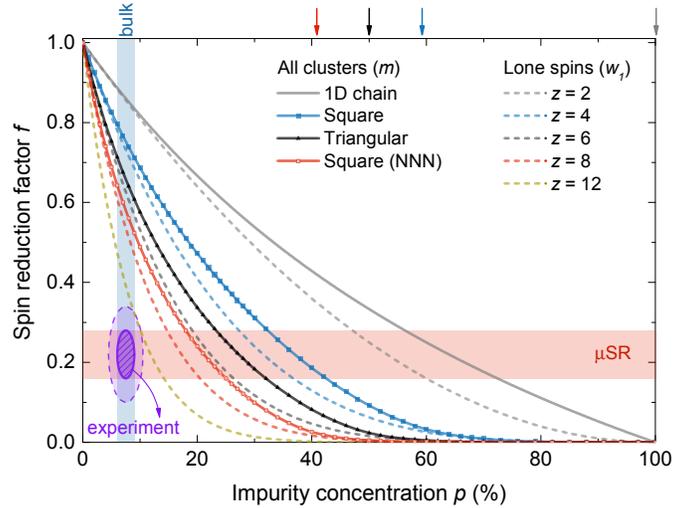
Supplementary Fig. 1 | Spin-reduction factor due to impurity clusters. The solid lines are the lower bounds $m(p)$ on the average-spin reduction factor $f(p) = \langle S \rangle / S$ given by Eq. (1) that were numerically calculated for various lattices and coordination numbers z. The coordination numbers of the lattices are: $z = 2$ for the 1D chain, $z = 4$ for the square lattice, $z = 6$ for the triangular lattice, and $z = 8$ for the square with additional next-nearest-neighbour (NNN) couplings. The $z = 2$ 1D-chain case is analytically solvable with exact cluster probabilities $w_s(p) = sp^{s-1}(1 - p)^2$ [1] that, by using Eq. (1), give an analytical result for the lower bound, $m(p) = (1 - p)/(1 + p)$. The dashed lines indicate the first term $w_1(p) = (1 - p)^z$ of the lower bound $m(p) \geq w_1(p)$ and correspond to the contribution from lone impurity spins. The arrows indicate percolation thresholds p_c for the corresponding lattices defined as the lowest impurity concentration above which the lattice contains an infinite spanning cluster with probability one [1]. The shaded blue region indicates the 1-sigma ($\sim 68\%$ confidence-level) experimental interval for the impurity concentration p [2], while the shaded red region indicates the 1-sigma experimental interval for the spin reduction factor $f(p)$ in Zn-brochantite (see the main text). The hashed violet region is the combined 1-sigma region consistent with experiment, while the dashed violet ellipse encloses the 2-sigma ($\sim 95\%$ confidence-level) experimental region. All the theoretical lower bounds for the impurity spin lie well above the 2-sigma experimental region, refuting these as possible impurity-only explanations of our experimental results on Zn-brochantite.

We stress that the lower bounds of Eq. (1) and Eq. (2) describe the lowest possible average impurity spin and derive from simple quantum spin addition rules in random impurity clusters. They and are thus independent of the specifics of the impurity–impurity couplings giving rise to these clusters. As such, they might not be saturated by any physically-sensible model of impurity–impurity couplings on a given lattice, and so we would actually expect $f(p) \gg m_S(p)$ to hold in real materials. Nevertheless, they represent the limiting scenario for average impurity spin reduction via impurity–impurity couplings (on a given impurity-site lattice and with a given distance-range for the couplings), and if found to be violated, categorically exclude this as a possible explanation for impurity magnetism in the system in question.

Comparison with experiment

In Zn-brochantite there are $S = 1/2$ impurities originating from Cu–Zn site-substitution disorder, where the spinful Cu^{2+} ions nominally form a 2D kagome lattice and the spinless Zn^{2+} ions nominally sit at the centres of the kagome-lattice hexagons [2]. As the Cu–Zn disorder in Zn-brochantite cannot introduce interlayer cou-

plings between kagome planes, its impurity-site lattice and its couplings are necessarily 2D, in contrast to the 3D impurity-site lattice proposed for the related quantum kagome antiferromagnet herbertsmithite [3]. Assuming only nearest-neighbour impurity–impurity couplings, the only two plausible impurity lattices in Zn-brochantite are therefore the triangular lattice (extra Cu^{2+} spin on Zn^{2+} sites) or the kagome lattice (missing Cu^{2+} spin due to extra Zn^{2+}). The former has a coordination number of $z = 6$, while the latter has $z = 4$. The observed concentration of spin-1/2 impurities in Zn-brochantite is relatively low at $p = 6$–9% [2], while the observed average magnetic moment per impurity 0.19–0.28μ_B (see the main text) corresponds to a strong average spin reduction factor of $f(p) = 0.16$–0.28, assuming a full impurity magnetic moment in the range 1.0–1.2μ_B typical for Cu^{2+} ions in an oxygen environment [4].

To compare this with the lower bound on the spin reduction factor $f(p)$, as given by Eq. (1) we performed numerical Monte–Carlo calculation of this lower bound $m(p)$ for a variety of impurity-site lattices with coordination numbers ranging from $z = 2$ to $z = 8$ and a range of p from zero to one (Supplementary Fig. 4). The simulation algorithm was similar to the Hoshen–Kopelman algorithm [5] and had a guaranteed space complexity of
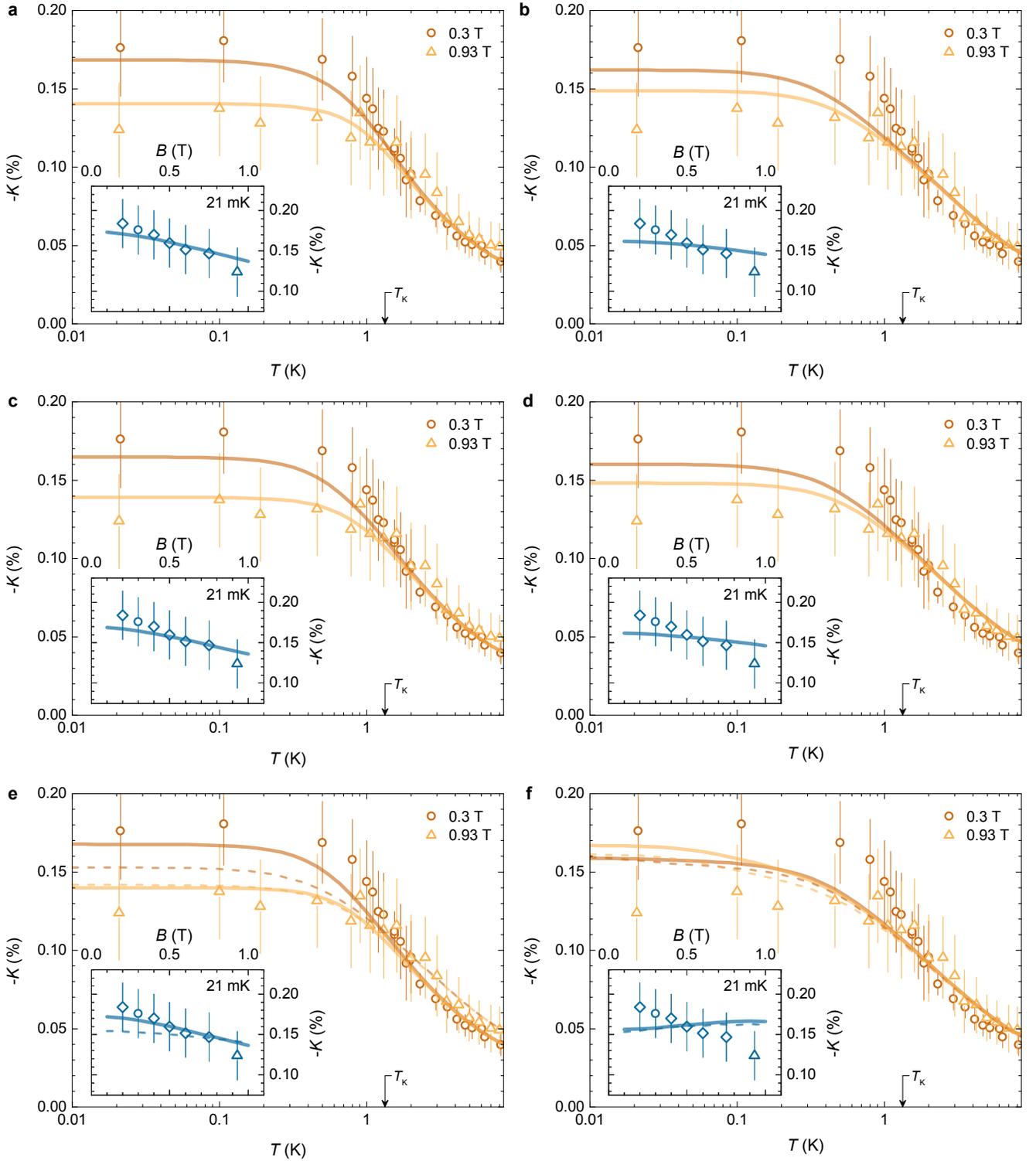
Supplementary Fig. 2 | Muon Knight shift. a-f, The Knight shift vs. temperature (main panels) and magnetic field (insets). The experimental data (symbols) are the same as in Fig. 2a in the main text while the theoretical curves (lines) are detailed below. **a**, NRG theoretical prediction computed for a "narrow" conduction band such that $T_K/D \approx 0.5$, where D is the half-bandwidth of the band. **b**, The effect of a finite spinon g-factor in a narrow conduction band, $T_K/D \approx 0.2$. **c**, NRG calculation for a triangular-shaped DOS in a narrow-band case with $T_K/D \approx 0.2$. **d**, The effect of potential scattering for $V/J = 0.5$, with all the other parameters being the same as in the reference model. **e**, The effect of the XXZ anisotropy in the Kondo exchange coupling for a dominant longitudinal (Ising) coupling (solid lines) and for a dominant transverse coupling (dashed lines). The magnetic field is oriented along the longitudinal z-axis. **f**, The effect of a reduced spinon density of states (DOS) around the spinon chemical potential due to spinon pairing with a hard gap (solid lines) and a BCS-like gap (dashed lines).
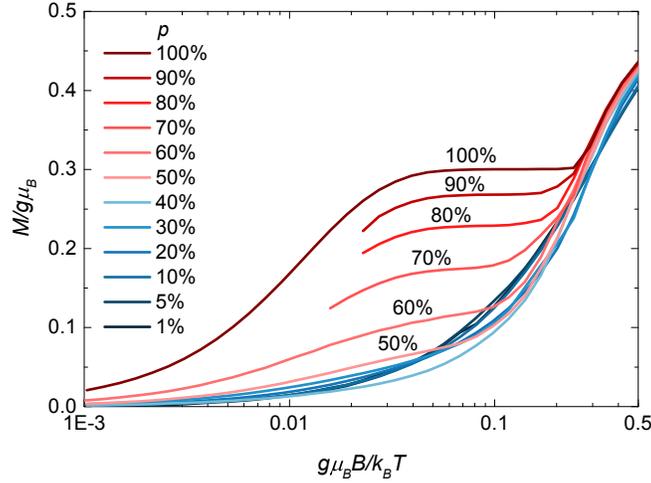
Supplementary Fig. 3 | Magnetization in the Kondo lattice model with a finite impurity concentration. The field dependence of the average impurity magnetization at $T = 0.01D$ for a broad range of impurity concentrations p. A magnetization plateau emerges above $p \sim n$, where n is the electron density in the lattice; here $n = 0.5$. At low impurity concentrations the curves are very similar. Therefore the experimentally-observed 10% impurity concentration in Zn-brochantite can still be considered within the dilute limit.
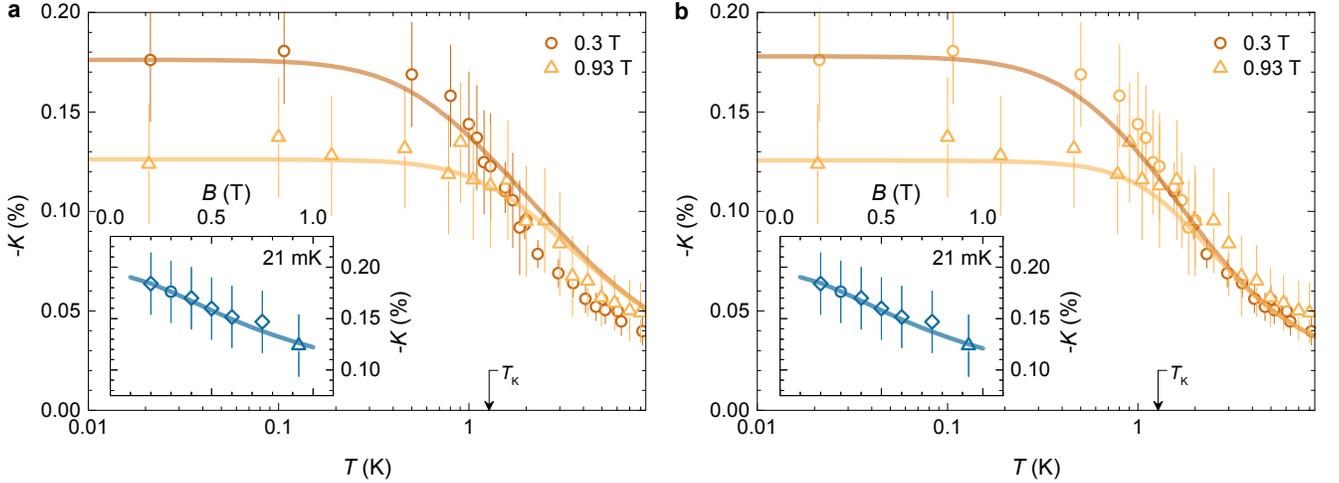
Supplementary Fig. 4 | Muon Knight shift. a, Hypothesis of the impurity g-factor $g = 6.5$ much in excess of the experimentally determined value of $g = 2.3(3)$. **b**, Hypothesis of a negative bulk g-factor, $g_{\text{bulk}} = -3$. Here $\rho J = 0.5$, so that $T_K/D \approx 0.2$. Better agreement at low temperatures comes at a price of worse agreement at high temperatures. This could be improved by taking a smaller value of J, but then $|g_{\text{bulk}}|$ would need to be even larger.

$O(L)$ for simulating an $L \times L$ patch of a 2D impurity lattice ($L = 4001$ in our case). Each simulation was run 5 times to estimate the statistical uncertainty of the results. The results conclusively show that the inequality $f(p) \geq m(p)$ of Eq. (1) is strongly violated in Zn-brochantite for all simulated lattices. Furthermore, at a $>95\%$ confidence level it must be violated for any lattice with $z \leq 12$, as we observe $f(p) < w_1(p)$ for those z, but $w_1(p) \leq m(p)$ for any lattice. This result is strong enough to also *a priori* exclude both a kagome impurity lattice with nearest-neighbour (NN) and next-nearest-neighbour (NNN) couplings ($z = 8$), as well as a triangular impurity

lattice with NN and NNN couplings ($z = 12$). We thus conclude that a model with only short-range impurity–impurity couplings between randomly-placed impurities is not compatible with the experimentally determined average impurity moment in Zn-brochantite.

Perturbations to the Conventional Kondo Model

The impurity magnetization $M(B,T)$ of the simple single-channel $S = 1/2$ Kondo model with an isotropic exchange coupling to a wide spinon band with a constant density of states — the "reference model" — does not
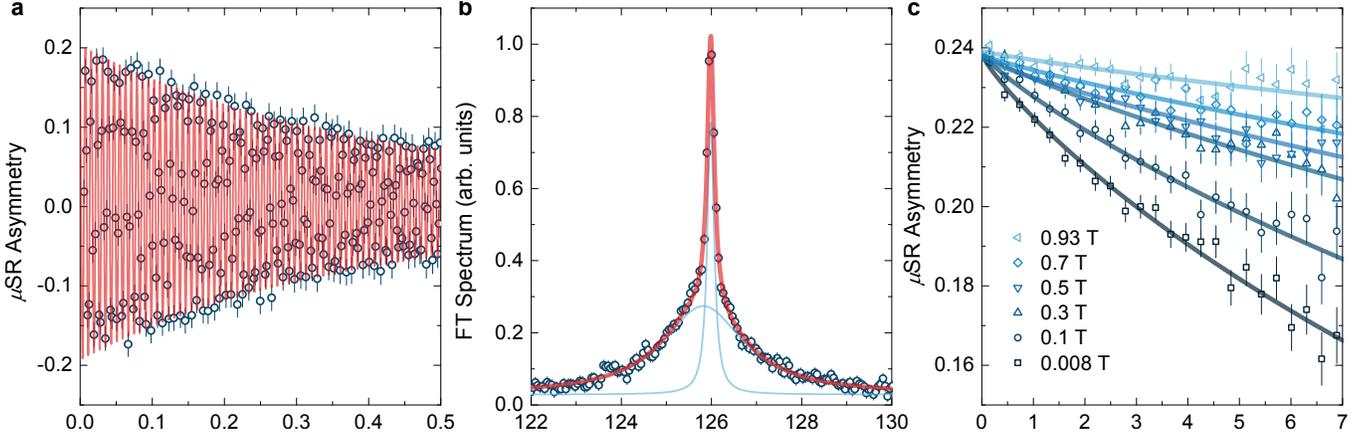
Supplementary Fig. 5 | Muon spin rotation and relaxation measurements. a, The oscillation of the μSR asymmetry in Zn-brochantite, measured in a 0.93 T transverse field at 21 mK (dots). The solid line shows a two-component fit with the model given by Eq. (1) in the main text. **b**, The corresponding Fourier transform of the μSR data (dots) and its fit with two Lorentzians (thick line). The two components, which are different in width and line position, are shown by thinner lines. The narrow (minor) one is the reference signal arising from muons that stop in the silver sample holder, while the broad (dominant) line is assigned to muons stopping in the sample. **c**, A collection of μSR asymmetry curves at 0.3 K measured in various longitudinal applied fields (symbols) and fitted with the model given by Eq. (3) in the main text (lines).

appear to fully match the measured muon Knight shift (see Fig. 2 in the main text). Therefore, a number of generalizations of the reference model were considered in our attempt to find a better quantitative agreement between theory and experiment (see Methods in the main text). These include narrow spinon bands, a finite spinon g factor, energy-dependent bands, potential Kondo scattering, an XXZ anisotropic Kondo coupling, and a band-gap opening. The effects of these perturbations on the Knight shift are summarized in Supplementary Fig. 5.

Furthermore, since the impurity concentration in Zn-brochantite is 6–9% [2], additional impurity–impurity interactions might represent important perturbations to the single-impurity Kondo model. Their effect on the impurity magnetization for the impurity concentration p spanning 1–100% is shown in Supplementary Fig. 6.

The field dependence of the measured Knight shift at low temperatures can be effectively accounted for by a renormalization of g factors. The effects of renormalizing the impurity and spinon g factors are shown in Supplementary Fig. 7.

SUPPLEMENTARY METHODS

μSR measurements

A typical muon spin rotation dataset measured in a transverse field of 0.93 T at a base temperature of 21 mK is shown in Supplementary Fig. 8a. The μSR asymmetry curve consists of two components (Eq. (1) in the main text), the dominant one with the amplitude $A_1 = 0.163(9)$ and the minor one with the ampli-

tude $A_2 = 0.036(3)$. Their corresponding frequencies are $\nu_1 = 125.821(15)$ MHz and $\nu_2 = 125.977(17)$ MHz. The dominant component exhibits exponential decay with a decay rate of $\lambda_1 = 2.2(2)$ μs, while the relaxation of the minor component is much slower, with $\lambda_2 = 0.09(3)$ μs. The two components are clearly seen in the Fourier transform (FT) spectrum of the same μSR dataset (Supplementary Fig. 8b). The FT spectrum can be fit with two Lorentzian lines with central frequencies ν_1 and ν_2. The broader, dominant line (in intensity) is notably shifted to lower frequencies with respect to the narrower minor line. The dominant component is thus assigned to the sample, while the minor component is assigned to the silver sample holder. This assignment is further reinforced by the fact that the frequency ν_2 is temperature independent, while the frequency ν_1 changes with temperature, giving a muon Knight shift that depends on temperature (see Fig. 2a in the main text).

A set of typical muon spin relaxation measurements in various longitudinal applied fields at the temperature of 0.3 K is shown in Supplementary Fig. 8c. A stretched-exponential model given by Eq. (3) in the main text was fit to each dataset. The initial muon asymmetry was found to be $A_1 + A_2 = 0.239(4)$, while the constant background signal was set to $A_2 = 0.053(3)$, so that the ration A_2/A_1 was the same as the one found in the muon spin rotation measurements.

* andrej.zorko@ijs.si

[1] Stauffer, D. *Introduction to percolation theory* (Taylor & Francis, London Bristol, Pennsylvania, 1994).

[2] Li, Y. *et al.* Gapless quantum spin liquid in the $S = 1/2$ anisotropic kagome antiferromagnet $ZnCu_3(OH)_6SO_4$. *New J. Phys.* **16**, 093011 (2014).

[3] Han, T.-H. *et al.* Correlated impurities and intrinsic spin liquid physics in the kagome material Herbertsmithite. *Phys. Rev. B* **94**, 060409(R) (2016).

[4] Abragam, A. *The Principles of Nuclear Magnetism* (Oxford University Press, Oxford, 1961).

[5] Hoshen, J. & Kopelman, R. Percolation and cluster distribution. I. Cluster multiple labeling technique and critical concentration algorithm. *Phys. Rev. B* **14**, 3438 (1976).